Asian Journal of Current Research in Clinical Cancer
ISSN: 3062-4444
2024, Volume 4, Issue 1, Page No: 61-78

Available online at: www.galaxypub.co/page/journals

Galaxy Publication

Galaxy Publication

Fibulin-5 (FBLN5) as an Independent Prognostic Indicator in Gastric Cancer: Clinical and Molecular Insights

I. Horvat[1*], J. Kovačević[1], D. Babić[1]

[1]Department of Cancer Immunology, School of Medicine, University of Zagreb, Zagreb, Croatia.

***E-mail** ✉ zagreb.immuno.57@protonmail.com

Received: 19 December 2023; **Revised:** 18 February 2024; **Accepted:** 18 March 2024

ABSTRACT

Aberrant expression of Fibulin-5 (FBLN5) has been implicated in multiple cancer types, yet its role in gastric cancer (GC) remains unclear. This study aimed to investigate the clinical and biological significance of FBLN5 in GC. Differential FBLN5 expression and its association with clinicopathological features were analyzed using data from The Cancer Genome Atlas-GC (TCGA-GC) and Gene Expression Omnibus (GEO) databases. The prognostic value of FBLN5 was evaluated using Kaplan–Meier survival analysis, and its functional roles were explored. Furthermore, a gastric cancer tissue microarray was constructed, and FBLN5 expression was validated through immunohistochemistry and Western blotting, confirming its overexpression in GC. High FBLN5 mRNA levels were associated with poor patient outcomes and showed significant correlations with INFc status and N3 lymph node metastasis. Both univariate and multivariate analyses identified FBLN5 expression and lymph node metastasis as independent prognostic factors, which were used to develop a nomogram for clinical application. Collectively, these findings indicate that FBLN5 overexpression is linked to adverse prognosis in GC, highlighting its potential as a prognostic biomarker.

Keywords: Gastric cancer, Prognosis, FBLN5, Fibroblast

How to Cite This Article: Horvat I, Kovačević J, Babić D. Fibulin-5 (FBLN5) as an Independent Prognostic Indicator in Gastric Cancer: Clinical and Molecular Insights. Asian J Curr Res Clin Cancer. 2024;4(1):61-78. https://doi.org/10.51847/ET9tKdX9nE

Introduction

Gastric cancer (GC) ranks as the second most common malignancy of the digestive tract and is the third leading cause of cancer-related mortality globally [1]. Due to low rates of early detection, approximately 70% of patients are diagnosed at advanced stages [2]. At this stage, tumor cells have often invaded blood vessels or lymphatics [3], allowing them to remain dormant and colonize distant tissues. Consequently, even after radical surgery, patients with lymph node metastasis exhibit a 20% recurrence rate at five years, while hematogenous metastasis can reach up to 40% [4].

The tumor microenvironment (TME) in GC is highly heterogeneous, involving dynamic interactions between cancer cells and stromal components. Fibroblasts, a key component of the TME, contribute to tumor angiogenesis [5], activate epithelial-mesenchymal transition (EMT), and modulate RAS and TGF-β signaling, which induces morphological changes in tumor cells and weakens cell-cell adhesion [6, 7]. This facilitates detachment of tumor cells from the primary site and promotes metastasis [8]. Additionally, fibroblasts influence immune cell infiltration, distribution, and phenotypes through chemokines (CXCL12, CXCL16), interleukins (IL6, IL8, IL11), and surface proteins such as PD-1/PD-L2, potentially suppressing antitumor immunity and enhancing metastatic potential [9].

Although fibroblast functions have been studied through bioinformatics and experimental approaches, the specific contributions of different fibroblast subtypes remain underexplored. The fibulin (FBLN) family, consisting of FBLN1–7, is broadly present in the extracellular matrix (ECM) and contributes to the assembly and stabilization of basement membranes, elastic fibers, and connective tissues [10, 11]. Unlike other family members, FBLN5

contains a conserved RGD motif that binds integrins, facilitating endothelial cell adhesion [12, 13]. FBLN5 is also critical for elastin polymer assembly and fiber interactions [14].

Functionally, FBLN5 regulates cell proliferation, motility, tumorigenesis, and tissue repair [15] and serves as a TGF-β target in fibroblasts and endothelial cells, influencing tumor progression [16, 17]. Its role in cancer appears context-dependent: FBLN5 can act as a tumor suppressor in ovarian [15], bladder [18], and lung cancers [19] by inducing cell cycle arrest, while promoting EMT and metastasis in breast [20], pancreatic [21], cervical [22], and gastric cancers [23, 24]. Prior studies have reported elevated FBLN5 expression in advanced GC, supporting proliferation and invasion, but its clinical relevance and mechanistic roles remain insufficiently characterized, motivating this study.

Materials and Methods

Patients and tissue samples

Tumor tissues, adjacent non-tumor tissues, and clinical data from 269 GC patients who underwent radical gastrectomy at Harbin Medical University (HMU) Cancer Hospital were collected to establish the HMU-GC cohort, with updates through December 2021. Written informed consent was obtained from all participants, and the study was approved by the Institutional Review Committee of HMU Cancer Hospital. The dataset was deposited in the GEO repository (GSE184336 and GSE179252). RNA extraction, library preparation, and mRNA sequencing were conducted by Novogene Biotech Co., Ltd. (Beijing, China).

Data processing

High-throughput sequencing data from TCGA-Stomach Adenocarcinoma (TCGA-STAD) and the HMU-GC cohort were normalized to transcripts per kilobase million (TPM) to account for gene length and sequencing depth. Batch effects due to non-biological variations were corrected using the ComBat algorithm (22257669) implemented in the "sva" package. The HMU-GC and TCGA-STAD datasets were merged to serve as a training cohort. For validation, microarray datasets GSE15459 and GSE62254 were retrieved from GEO, and raw CEL files were processed to obtain absolute mRNA expression values, followed by ComBat correction for batch effects.

Bioinformatics analyses

In the training cohort, patients were categorized into high- and low-FBLN5 expression groups based on the median mRNA expression level. Principal component analysis (PCA) was performed using z-score normalization across the expression profile, followed by dimension reduction with the prcomp function to generate a reduced data matrix. Differentially expressed genes (DEGs) between high- and low-expression groups were identified using the limma package, applying a $|\log2 \text{ fold change}| > 2$, $p < 0.05$, and false discovery rate (FDR) correction.

Gene Ontology (GO) enrichment analysis was performed using annotations from the org.Hs.eg.db package, covering biological processes (BP), cellular components (CC), and molecular functions (MF). For Kyoto Encyclopedia of Genes and Genomes (KEGG) pathway analysis, the latest pathway annotations were retrieved via the KEGG REST API (https://www.kegg.jp/kegg/rest/keggapi.html), and enrichment analysis was conducted using the clusterProfiler package (assessed 7 April 2022). Gene Set Enrichment Analysis (GSEA) was also performed with clusterProfiler to identify pathways enriched in the high-expression group, using the hallmark gene sets as reference and thresholds of |normalized enrichment score (NES)| > 1, nominal $p < 0.05$, and FDR $q < 0.25$.

A protein–protein interaction (PPI) network was constructed using STRING (version 11.5) with a minimum interaction score of 0.9 (assessed 10 November 2021). Receiver operating characteristic (ROC) curves were generated using the pROC and timeROC packages, and visualized with ggplot2. Immune infiltration analysis was performed using CIBERSORT and TIMER algorithms, while the ESTIMATE algorithm assessed immune and stromal cell content, yielding immune scores, stromal scores, and tumor purity estimates. Somatic mutation data from TCGA-STAD were obtained via the GDCquery_Maf() function (mutect2 pipeline) of the TCGAbiolinks package, with mutation frequencies visualized using maftools. Chemotherapy sensitivity was evaluated using the PRISM database, and immunotherapy efficacy was assessed via the TIDE database (http://tide.dfci.harvard.edu; assessed 11 June 2021). EMT scores for each tumor sample were computed using single-sample GSEA (ssGSEA). Nomograms and calibration curves were created using the rms and survival packages, and decision curve analysis (DCA) was performed using the stdca.R script. Analyses were performed with Sangerbox 3.0 (version 1.1.3) [25].

Immunohistochemistry

A total of 180 GC tissue samples from Harbin Medical University Cancer Hospital were used to construct a tissue microarray. Sections were baked at 62 °C for 2 h, deparaffinized in xylene, dehydrated in alcohol, and subjected to antigen retrieval in EDTA buffer (pH 7.4) at 120 °C for 3 min, followed by natural cooling. Endogenous peroxidase activity was blocked using 0.3% hydrogen peroxide in methanol for 30 min, and slides were rinsed three times with PBS. Sections were blocked with goat serum at room temperature for 1 h and then incubated overnight at 4 °C with rabbit polyclonal anti-FBLN5 antibody (ABclonal, 1:150). Secondary antibody incubation was performed for 40 min at room temperature, followed by color development using diaminobenzidine (DAB). Sections were counterstained with hematoxylin and blued with ammonia. Two pathologists independently scored FBLN5 staining using a semiquantitative H-score (0–300), calculated as the product of staining intensity (0–3) and percentage of positive area. Expression was dichotomized into high or low groups according to X-tile software based on survival data.

Western blotting

Cell lines (GES, AGS, BGC-823, HGC-27, and MKN-28) were lysed on ice in RIPA buffer containing protease and phosphatase inhibitors for 30 min, followed by centrifugation at 13,000 rpm for 15 min. Supernatants were collected, mixed with 5× loading buffer, and heated at 100 °C for 10 min. Protein concentrations were quantified using the BCA assay (Thermo Scientific). Proteins were separated on 12% SDS-PAGE gels, transferred to PVDF membranes, and blocked with 5% skim milk for 2 h. Membranes were incubated overnight at 4 °C with primary antibodies against FBLN5 (1:1000) and β-Tubulin (1:1000; ABclonal), followed by 1 h incubation with HRP-conjugated secondary antibody (1:5000). Protein bands were visualized using ECL detection. Experiments were performed in triplicate.

Statistical Analyses

All statistical analyses were conducted using SPSS version 25.0. Continuous variables were compared using the Kruskal–Wallis test, whereas categorical variables were analyzed with the Chi-square test to examine associations between FBLN5 mRNA or protein expression and clinicopathological features. The Cox proportional hazards model, implemented via the survival package, was used to estimate hazard ratios (HRs) and 95% confidence intervals (CIs). Kaplan–Meier curves were generated for survival analysis, and statistical significance was defined as a two-tailed p-value < 0.05.

Results and Discussion

Association of FBLN5 expression with prognosis and clinicopathological features

Patients were stratified into high- and low-FBLN5 expression groups based on the median mRNA level. Principal component analysis (PCA) confirmed both inter-group and intra-group consistency between the two cohorts **(Figure 1a).** Survival analysis revealed that patients with high FBLN5 expression exhibited significantly poorer outcomes, with a median overall survival (OS) of 33.03 months compared to 68.37 months in the low-expression group ($p < 0.001$; HR: 1.60, 95% CI: 1.25–2.05) **(Figure 1b)**.

This prognostic trend was validated in an independent cohort, where patients in the high-expression group also showed reduced survival ($p < 0.001$; HR: 0.63, 95% CI: 0.49–0.81) **(Figure 1c)**. Analysis of TCGA data further demonstrated that high FBLN5 expression was associated with worse disease-specific survival (DSS) **(Figure 1d)** and progression-free interval (PFI) **(Figure 1e)**.

Comparisons between tumor tissues and adjacent non-tumor tissues in the training cohort indicated that FBLN5 was upregulated in gastric cancer cells **(Figure 1f)**. Examination of clinicopathological correlations revealed no significant associations between FBLN5 expression and sex or M stage. In contrast, FBLN5 expression was significantly correlated with T stage ($p < 0.001$, **(Figure 1g)**), N stage ($p < 0.001$) **(Figure 1h)**, and overall pTNM stage ($p < 0.001$) **(Figure 1i)**.

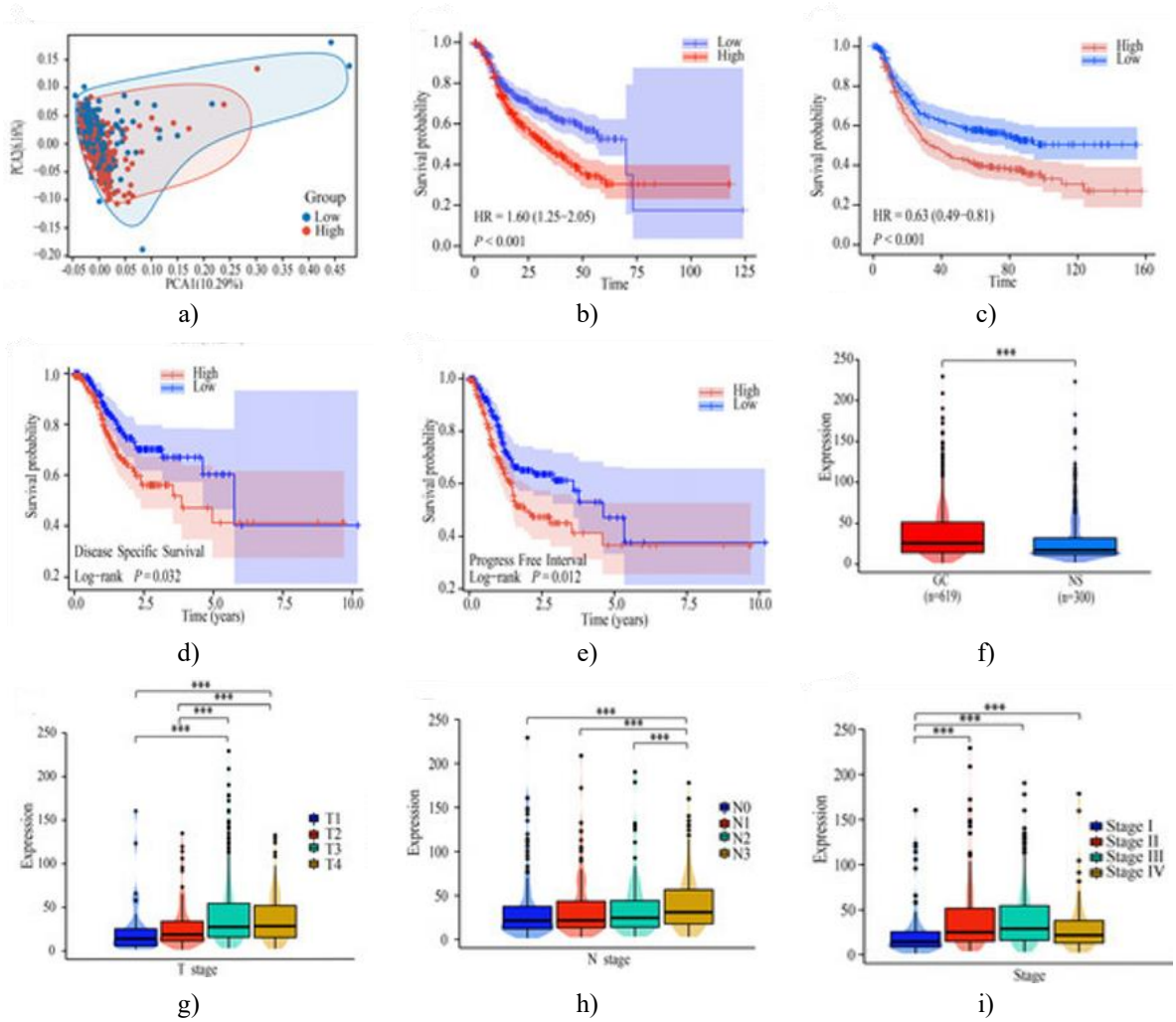

Figure 1. Relationship between FBLN5 Expression and Prognostic/Clinicopathological Features (a) Principal component analysis (PCA) showing the distribution of patients according to high versus low FBLN5 expression. (b) Kaplan–Meier survival curves comparing overall survival (OS) between high- and low-FBLN5 expression groups in the HMU-TCGA cohort ($p < 0.001$). (c) OS comparison in the GEO cohort ($p < 0.001$). (d) Disease-specific survival (DSS) stratified by FBLN5 levels ($p < 0.05$). (e) Progression-free interval (PFI) analysis by FBLN5 expression ($p < 0.05$). (f) Comparison of FBLN5 expression in gastric cancer tissues (n = 619) versus adjacent non-tumorous tissues (n = 300). (g–i) Expression patterns of FBLN5 across different tumor stages ($p < 0.05$). *** $p < 0.001$. Abbreviations: HMU, Harbin Medical University; TCGA, The Cancer Genome Atlas; GEO, Gene Expression Omnibus; GC, gastric cancer; DSS, disease-specific survival; PFI, progression-free interval.

Functional characterization of FBLN5 in gastric cancer

Differential gene expression analysis comparing high- versus low-FBLN5 expression identified 2,663 genes upregulated and 5,957 downregulated **(Figure 2a)**. Functional enrichment analysis indicated that these genes participate in critical biological processes including system development, regulation of cellular activity, cell differentiation, signal transduction, phosphorus metabolism, and responses to chemical stimuli **(Figure 2b)**. In terms of cellular localization, enrichment was observed in the cytosol, nuclear components, and vascular structures **(Figure 2c)**. Molecular function analysis revealed roles in cytoskeletal and transcription factor binding, cell adhesion interactions, and small GTPase activity **(Figure 2d)**.

KEGG pathway analysis highlighted significant involvement of FBLN5-related genes in MAPK, Rap1, and cGMP-PKG signaling pathways **(Figure 2e)**. Gene set enrichment analysis (GSEA) further revealed that high FBLN5 expression is associated with activation of epithelial-mesenchymal transition (EMT), TGF-β signaling, apoptosis, hypoxia, and angiogenesis pathways **(Figure 2f)**.

Protein–protein interaction (PPI) network analysis identified close interactions between FBLN5 and LOX family members (LOX, LOXL1–4) as well as ELN **(Figure 2g)**. Prognostic relevance of these PPI-associated genes was evaluated using ROC analysis **(Figures 3a–3g)**, indicating limited predictive power when considered individually. Multivariate Cox regression pinpointed FBLN5, ELN, and LOX as key prognostic markers. A composite prognostic score combining these three genes provided improved survival prediction compared to single-gene assessments **(Figure 3h)**. Kaplan–Meier analysis demonstrated that patients with higher combined risk scores exhibited significantly poorer overall survival **(Figure 3i).**

A risk factor plot illustrated the contribution of FBLN5, ELN, and LOX expression to patient prognosis **(Figure 3j)**. Incorporating this risk score with traditional clinicopathological variables in a multivariate Cox model enabled the construction of a prognostic nomogram **(Figure 3k)**. ROC curve analysis confirmed that combining the risk score with pTNM stage and patient age enhanced the ability to predict outcomes in gastric cancer patients **(Figure 3l).**

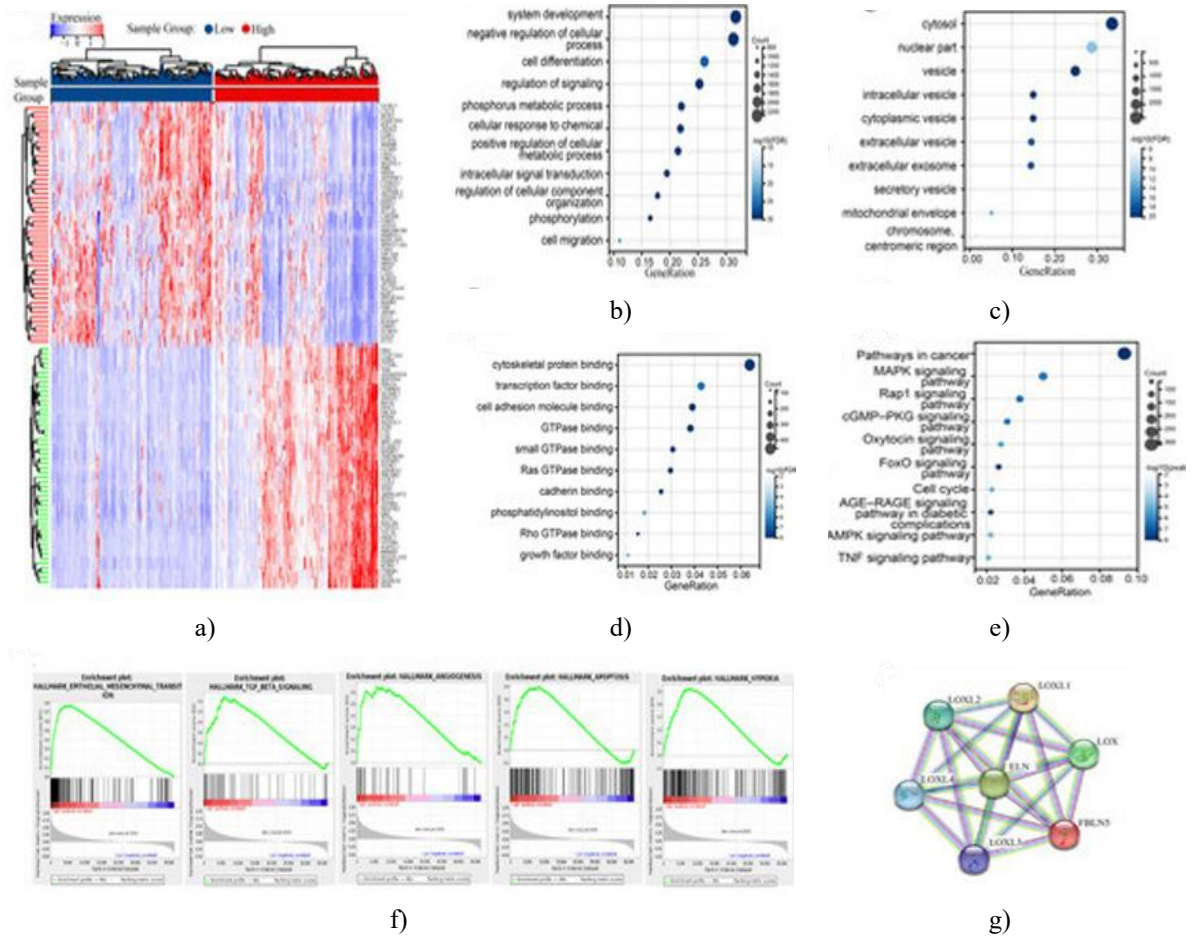

Figure 2. Functional characterization of FBLN5 in gastric cancer.
(a) Volcano plot depicting differentially expressed genes between high- and low-FBLN5 expression groups as determined using the "limma" package. GO enrichment analysis of FBLN5-related genes in the TCGA-GC dataset highlighting: (b) associated biological processes (BP), (c) cellular component (CC) localization, and (d) molecular functions (MF). (e) KEGG pathway enrichment analysis showing key signaling pathways linked to FBLN5 expression. (f) Gene set enrichment analysis (GSEA) of the high-FBLN5 expression group revealing significant enrichment of hypoxia, angiogenesis, TGF-β signaling, epithelial–mesenchymal transition (EMT), and apoptosis pathways (|NES| > 1, nominal $p < 0.05$, FDR $q < 0.25$). (g) Protein–protein interaction (PPI) network depicting proteins closely interacting with FBLN5

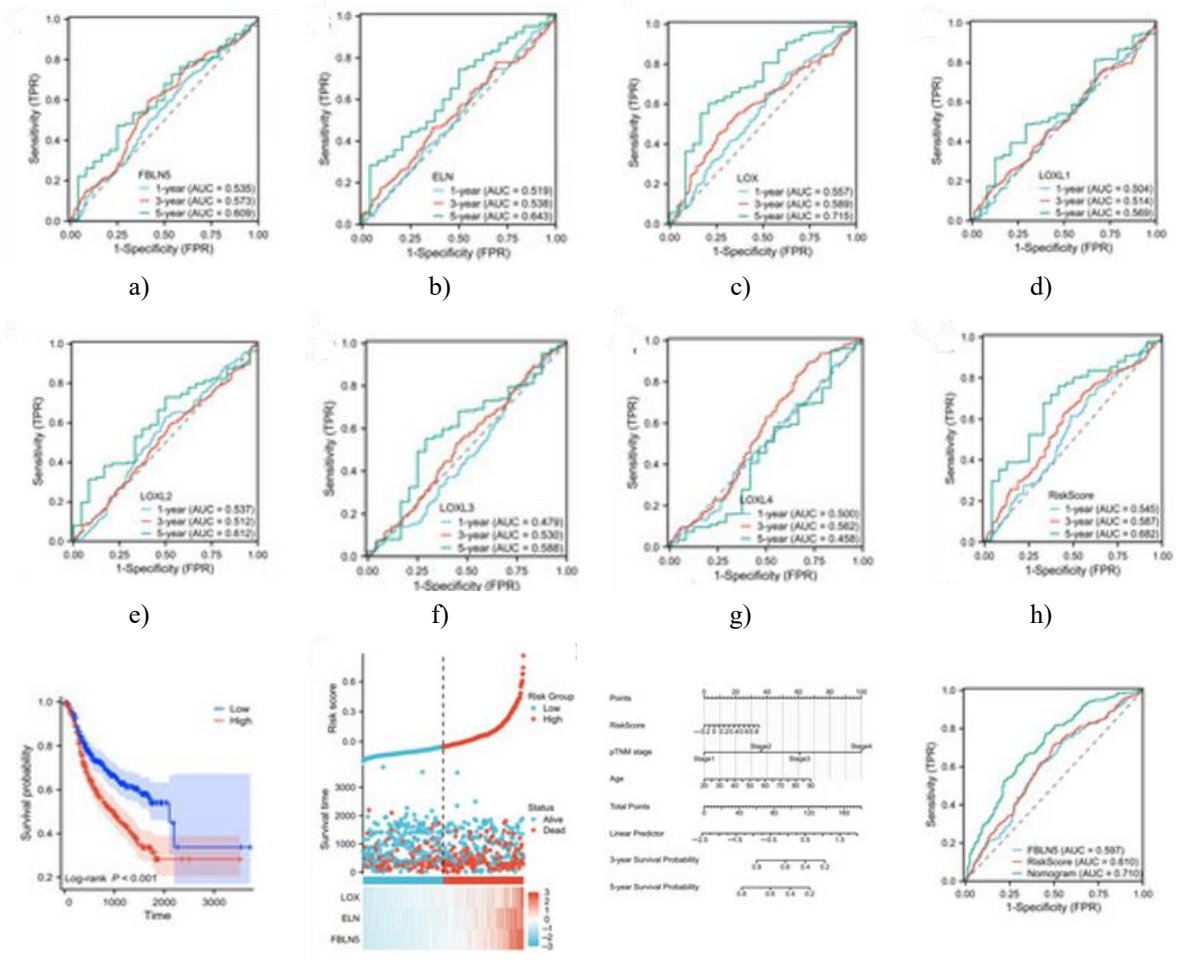

Figure 3. Prognostic evaluation of gastric cancer using FBLN5-associated gene expression**.** (a–g) ROC curves assessing the prognostic performance of individual mRNA levels of FBLN5, ELN, LOXL1, LOXL2, LOXL3, and LOXL4. (h) Combined prognostic risk score calculated from FBLN5, ELN, and LOX expression levels. (I) Kaplan–Meier survival analysis of patients stratified by the prognostic risk score. (j) Visualization of risk factor trends within the prognostic model. (k) Nomogram integrating the prognostic risk score with pTNM stage and patient age to predict overall survival. (l) ROC curves comparing the predictive accuracy of FBLN5 expression alone, the combined risk score, and the nomogram model. (OS, overall survival).

FBLN5 expression and immune microenvironment in gastric cancer

To explore the impact of FBLN5 on the tumor immune landscape, we analyzed its association with immune cell infiltration. Using the CIBERSORT algorithm, we observed that higher FBLN5 expression was linked to increased infiltration of several immune populations, including CD4+ T cells, natural killer (NK) cells, M0 and M2 macrophages, and mast cells (all $p < 0.05$) **(Figure 4a)**. TIMER analysis further confirmed significant positive correlations between elevated FBLN5 levels and the presence of CD4+ and CD8+ T cells, neutrophils, macrophages, and dendritic cells (all $p < 0.05$) **(Figure 4b)**. Additionally, tumors with high FBLN5 expression demonstrated elevated ESTIMATE scores, as well as higher immune and stromal scores, while showing reduced tumor purity (all $p < 0.05$) **(Figures 4c–4f)**. These findings indicate that FBLN5 may strongly influence the immune composition of the tumor microenvironment, potentially affecting immune surveillance and tumor progression.

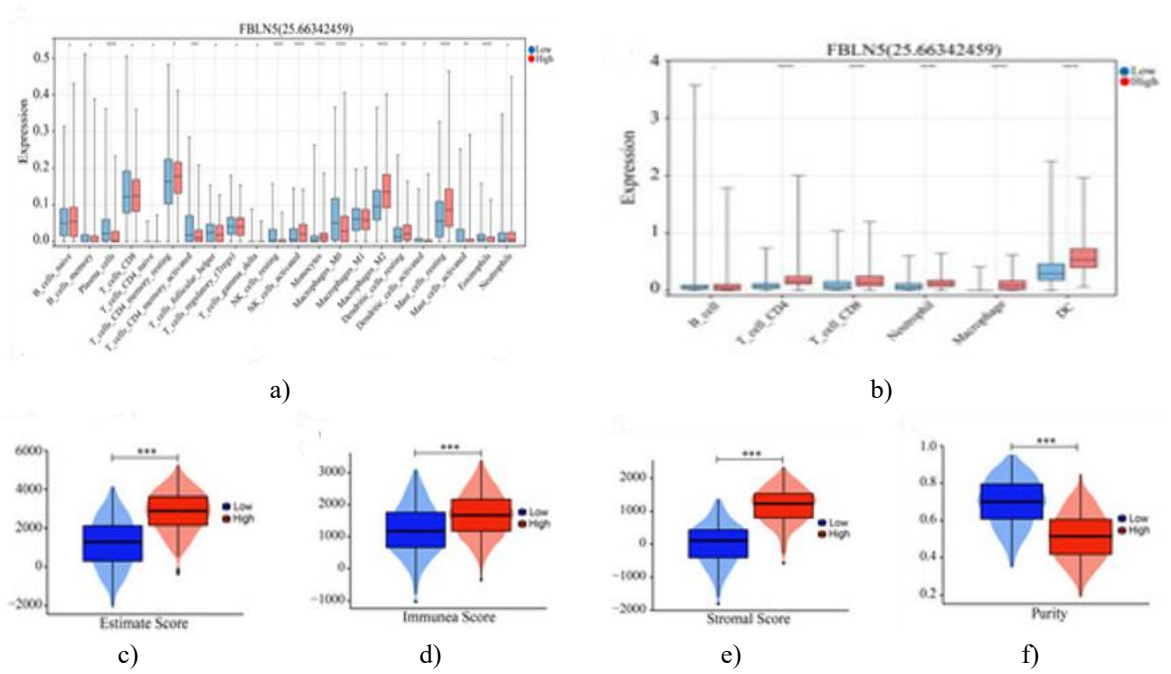

a) b) c) d) e) f)

Figure 4. FBLN5 Expression and Immune Features in Gastric Cancer
(a) Immune cell infiltration was estimated using the CIBERSORT algorithm to explore the relationship between FBLN5 expression and the abundance of immune cells in tumor samples. (b) TIMER analysis further examined correlations between FBLN5 levels and immune cell populations. (c) The ESTIMATE algorithm assessed the overall immune and stromal cell content in tumors. Panels (d–f) show the derived immune score, stromal score, and tumor purity, respectively. Significance levels are indicated as *p < 0.05, **p < 0.01, ***p < 0.001, ****p < 0.0001.

FBLN5 and tumor progression in gastric cancer

We next explored the potential role of FBLN5 in tumor progression and therapeutic response. Drug sensitivity analyses revealed that FBLN5 expression influenced patient responses to capecitabine, cisplatin, and oxaliplatin, whereas no significant effect was observed for irinotecan, 5-fluorouracil, docetaxel, or paclitaxel **(Figure 5a)**. Additionally, the predictive value of FBLN5 for immune checkpoint inhibitor response was evaluated **(Table 1)**. Notably, tumors with elevated FBLN5 levels exhibited significantly higher EMT scores compared with tumors expressing low FBLN5, suggesting that high FBLN5 may facilitate GC cell detachment and metastatic dissemination via EMT **(Figure 5b)**. Exon-level missense mutation analyses from TCGA-STAD data indicated a low mutation frequency of FBLN5 in the high-expression group **(Figure 5c)**, suggesting that FBLN5 maintains a stable regulatory role in advanced GC and is closely associated with disease progression.

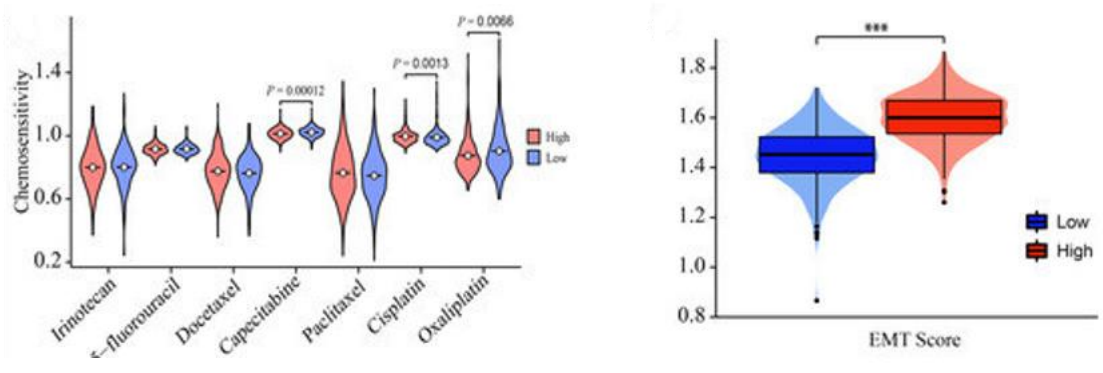

a) b)

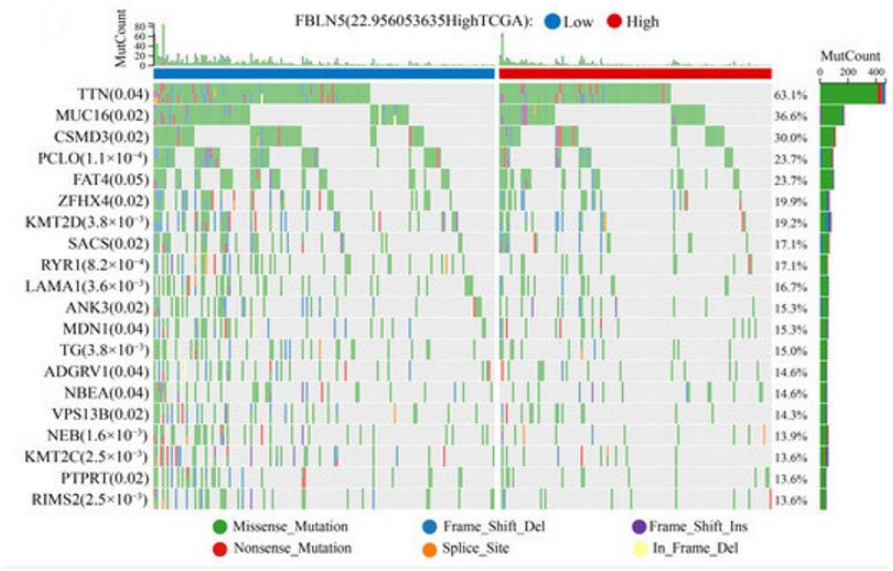

c)

Figure 5. Relationships between FBLN5 and tumor progression. (a) Chemotherapy analysis based on FBLN5 expression levels. (b) EMT score. (c) Mutations in FBLN5 during the regulation of cancer progression. *** p < 0.001.

Table 1. The values of FBLN5 to assess the sensitivity of immunotherapy checkpoints (TIDE).

Study	Cancer Type	Treatment	Pos/Neg Cases	AUC of			
				FBLN5	CD274	CD8	TMB
Zhao 2019	Glioblastoma	PD1_Pre	8/7	0.38	0.68	0.50	n/a
		PD1_Post	6/3	0.17	0.61	0.67	n/a
VanAllen 2015	Melanoma	CTLA4	19/23	0.48	0.64	0.70	0.67
Uppaluri 2020	HNSC	PD1_Pre	8/15	0.37	0.69	0.58	n/a
		PD1_Post	9/13	0.23	0.70	0.48	n/a
Ruppin 2021	NSCLC	PD1	7/15	0.59	0.70	0.75	n/a
Riaz 2017	Melanoma	PD1_Prog	4/22	0.80	0.52	0.91	0.57
		PD1_Naive	6/19	0.54	0.27	0.43	0.62
Prat 2017	NSCLC/HNSC/Melanoma	PD1	21/12	n/a	0.58	0.56	n/a
Nathanson 2017	Melanoma	CTLA4_Pre	4/5	0.15	0.66	0.50	n/a
		CTLA4_Post	4/11	0.57	0.66	0.77	n/a
Miao 2018	Kidney	ICB	20/13	0.67	0.42	0.47	0.65
McDermott 2018	Kidney	PD-L1	20/61	0.60	0.62	0.66	0.54
Mariathasan 2018	Bladder_mUC	PD-L1	68/230	0.42	0.58	0.60	0.78
Liu 2019	Melanoma	PD1_Prog	16/31	0.56	0.56	0.58	n/a
		PD1_Naive	33/41	0.39	0.51	0.47	n/a
Lauss 2017	Melanoma	ACT	10/15	0.69	0.78	0.71	0.76
Kim 2018	Gastric	PD1	12/33	0.19	0.88	0.80	n/a
Hugo 2016	Melanoma	PD1	14/12	0.28	0.60	0.49	0.68
Hee 2020	NSCLC_Oncomine	PD1	9/12	n/a	0.45	0.56	n/a
Gide 2019	Melanoma	PD1	19/22	0.47	0.88	0.86	n/a
		PD1 + CTLA4	21/11	0.52	0.79	0.74	n/a
Chen 2016	Melanoma	PD1_Prog	6/9	n/a	0.54	0.61	n/a
		CTLA4	5/11	n/a	0.42	0.67	n/a
Braun 2020	Kidney	PD1	201/94	0.58	0.56	0.60	0.56

TIDE, tumor immune dysfunction, and exclusion.

FBLN5 expression and its prognostic implications in gastric cancer

To investigate the prognostic relevance of FBLN5 in GC, we conducted immunohistochemical (IHC) staining using a tissue microarray **(Figure 6a)**. FBLN5 was primarily localized in the cytoplasm of tumor cells and in stromal fibroblasts. Interestingly, its distribution varied between high- and low-expression groups. In well-differentiated adenocarcinomas, FBLN5 exhibited strong cytoplasmic staining in both cancer cells and interstitial fibroblasts, whereas poorly differentiated adenocarcinomas showed heterogeneous expression, with some tumors exhibiting low levels in cancer cells but high expression in stromal fibroblasts. Mucinous adenocarcinomas displayed elevated FBLN5 in both compartments.

Kaplan–Meier survival analysis demonstrated that patients with lower FBLN5 expression had significantly improved overall survival compared to those with high expression ($p < 0.05$; HR = 2.40, 95% CI: 1.10–5.21) **(Figure 6b)**. Consistently, western blot analysis revealed that FBLN5 levels were markedly higher in GC cell lines compared to normal gastric epithelial cells, supporting a potential association with tumor histology **(Figure 6c).**

Univariate and multivariate Cox regression analyses identified FBLN5 expression and lymph node metastasis as independent predictors of patient prognosis ($p < 0.05$) **(Table 2)**. Chi-square analysis further revealed that high FBLN5 expression correlated with the INFc tumor infiltration pattern and advanced nodal stage (N3) **(Table 3)**. Based on these findings, a prognostic nomogram was constructed incorporating FBLN5 expression and other clinicopathological factors **(Figure 6d)**. Patients were stratified into high- and low-risk groups according to median nomogram scores, with the high-risk group showing shorter survival **(Figure 6e)**.

The predictive performance of the nomogram was evaluated using time-dependent ROC curves, with one-, two-, and three-year areas under the curve (AUCs) of 0.751 (0.564–0.938), 0.769 (0.647–0.891), and 0.733 (0.612–0.855), respectively **(Figure 6f)**. Calibration analysis yielded a concordance index (C-index) of 0.705 (0.659–0.752) **(Figure 6g)**, while decision curve analysis (DCA) demonstrated that combining FBLN5 expression with lymph node metastasis enhanced the accuracy of survival prediction and offered improved clinical utility **(Figure 6h).**

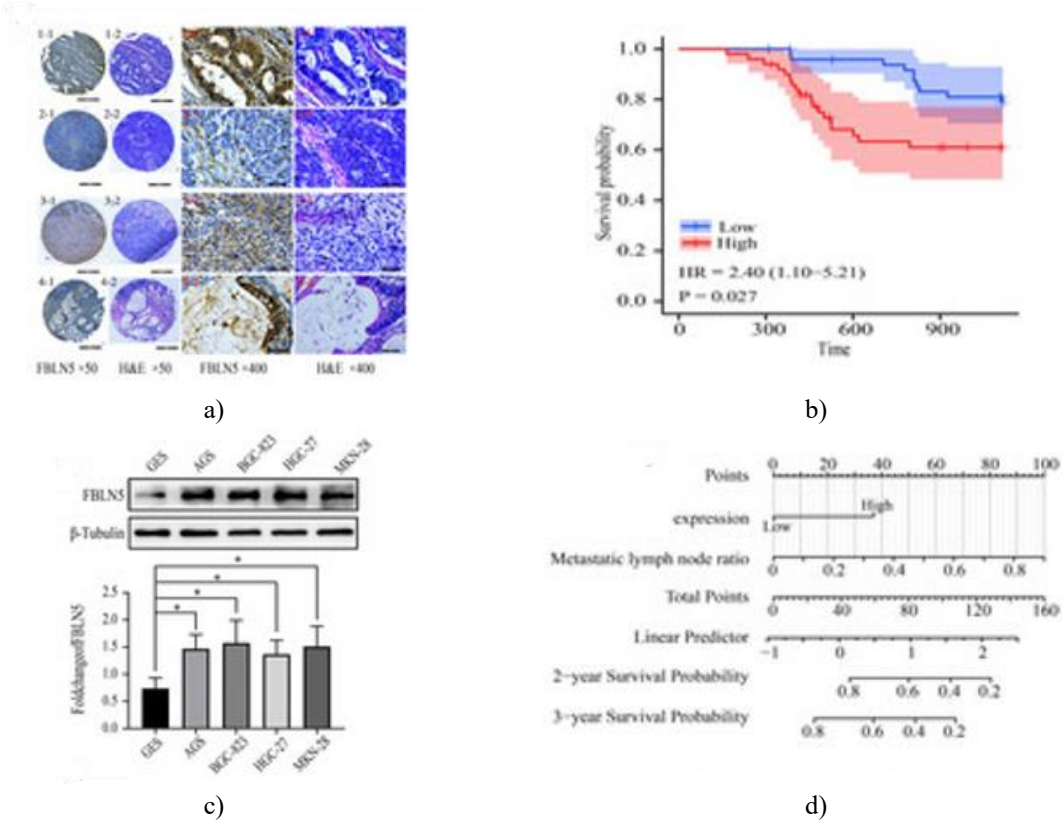

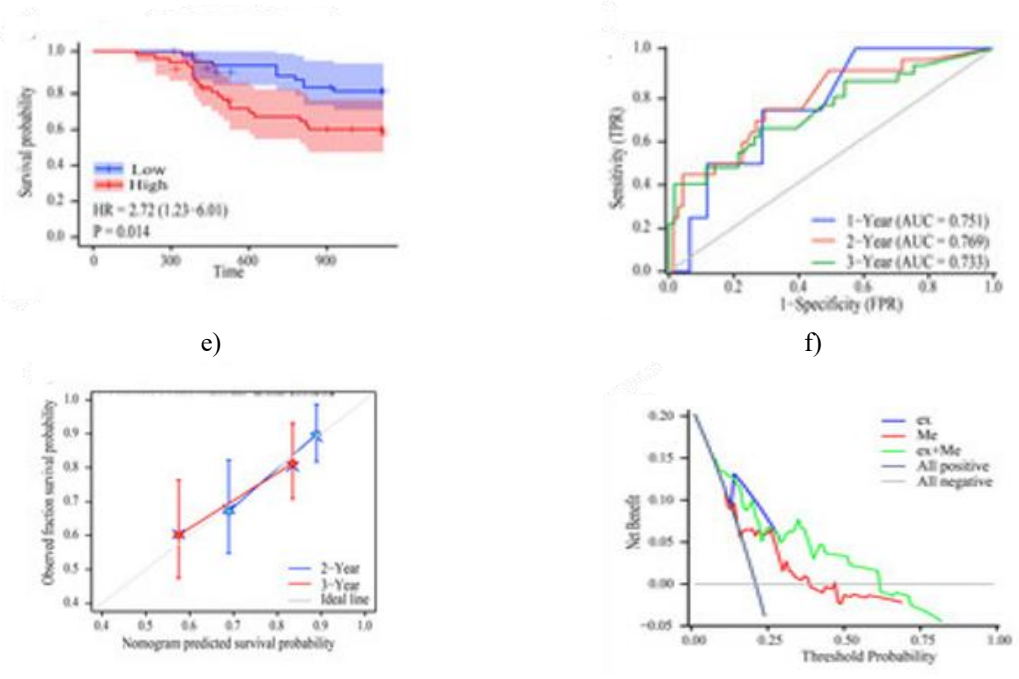

e) f)

g) h)

Figure 6. Evaluation of FBLN5 expression and development of a prognostic model.
(a) Immunohistochemical staining and H&E analysis of GC tissue microarrays at ×50 and ×400 magnification. (A1) Well-differentiated adenocarcinoma with strong FBLN5 expression in both tumor cell cytoplasm and interstitial fibroblasts. (A2) Poorly differentiated adenocarcinoma showing low FBLN5 in tumor cells but high expression in stromal fibroblasts. (A3) Another poorly differentiated adenocarcinoma with high FBLN5 expression. (A4) Mucinous adenocarcinoma exhibiting high FBLN5 levels in both tumor cytoplasm and interstitial fibroblasts.
(b) Kaplan–Meier survival curves comparing OS between high- and low-FBLN5 expression groups.
(c) FBLN5 protein levels in normal gastric epithelial and various GC cell lines (mean ± s.d., n = 3).
(d) Nomogram constructed to predict prognosis based on FBLN5 expression and lymph node metastasis status.
(e) Survival analysis stratified by the nomogram-derived risk scores.
(f) ROC curve assessing the predictive performance of the nomogram.
(g) Calibration plots evaluating two- and three-year survival prediction accuracy.
(h) Decision curve analysis (DCA) demonstrating the clinical benefit of combining FBLN5 expression with lymph node metastasis for prognosis prediction.
* $p < 0.05$.

Table 2. Cox univariate and multivariate analyses of FBLN5 gene expression.

Characteristics	Total (N)	Univariate Analysis		Multivariate Analysis	
		Hazard Ratio (95% CI)	p Value	Hazard Ratio (95% CI)	p Value
FBLN5 expression	100				
Low	50	Reference			
High	50	2.396 (1.102–5.205)	0.027	2.558 (1.162–5.632)	0.020
Sex	100				
Male	72	Reference			
Female	28	0.851 (0.362–2.002)	0.712		
Age	100	0.992 (0.957–1.028)	0.646		
BMI	100	0.944 (0.845–1.054)	0.303		
Tumor infiltration pattern	100				
INFa	20	Reference			
INFb	16	1.484 (0.371–5.937)	0.577		
INFc	48	1.761 (0.584–5.311)	0.315		
N/A	16	1.823 (0.489–6.790)	0.371		

Lymphatic infiltration	100				
Negative	55	Reference			
Positive	45	0.940 (0.445–1.988)	0.872		
Venous infiltration	100				
Negative	70	Reference			
Positive	30	0.592 (0.240–1.460)	0.255		
Nerve infiltration	100				
Negative	25	Reference			
Positive	75	2.243 (0.778–6.471)	0.135		
T stage	100				
T1	4	Reference			
T2	13	0.595 (0.054–6.565)	0.672		
T3	45	1.009 (0.130–7.821)	0.993		
T4	38	1.709 (0.225–12.999)	0.605		
pTNM stage	100				
I	10	Reference			
II	32	2.155 (0.259–17.902)	0.477		
III	58	4.558 (0.613–33.907)	0.138		
Metastatic lymph node ratio	100	14.056 (3.348–59.004)	<0.001	7.133 (1.241–41.011)	0.028
Borrmann type	100				
I	7	Reference			
II	19	0.291 (0.041–2.068)	0.217		
III	68	1.003 (0.236–4.270)	0.997		
IV	6	1.214 (0.171–8.621)	0.847		
Post-operative chemotherapy	100				
Without	97	Reference			
With	3	1.211 (0.164–8.915)	0.851		
Tumor location	100				
Lower third	54	Reference			
Middle and Upper third	42	1.866 (0.847–4.113)	0.122	1.589 (0.676–3.734)	0.289
Entire stomach	4	7.426 (2.017–27.337)	0.003	2.869 (0.565–14.569)	0.204
Histological type	100				
Well to moderately differentiated	46	Reference			
Poorly differentiated	26	0.592 (0.215–1.629)	0.310		
Signet ring cell	20	1.126 (0.459–2.764)	0.795		
Mucinous	8	0.323 (0.043–2.447)	0.274		
HER2 expression	100				
Positive	18	Reference			
Negative	82	0.602 (0.256–1.418)	0.246		
CEA	100				
≤5 ng/mL	86	Reference			
>5 ng/mL	14	0.679 (0.205–2.250)	0.526		
CA-199	100				
≤37 U/mL	88	Reference			
>37 U/mL	12	1.745 (0.663–4.593)	0.260		
CA724	100				
≤6 U/mL	74	Reference			
>6 U/mL	26	1.096 (0.483–2.490)	0.826		
FBLN5	619	1.004 (1.001–1.007)	<0.01	1.003 (0.998–1.007)	0.235
ELN	619	1.002 (1.000–1.003)	<0.05	1.000 (0.998–1.003)	0.698
LOX	619	1.005 (1.001–1.009)	<0.05	1.003 (0.998–1.008)	0.197
LOXL1	619	1.004 (0.999–1.009)	0.096		
LOXL2	619	1.002 (0.997–1.006)	0.499		
LOXL3	619	1.030 (0.992–1.069)	0.121		
LOXL4	619	1.012 (0.999–1.025)	0.062		<0.05
RiskScore	619	2.718 (1.444–5.116)	<0.01	2.226 (1.139–4.353)	

pTNM stage	605		<0.001		
Stage 1	81	Reference		Reference	<0.01
Stage 2	160	2.691 (1.395–5.191)	<0.01	2.491 (1.287–4.823)	<0.001
Stage 3	312	4.854 (2.633–8.947)	<0.001	4.645 (2.510–8.596)	<0.001
Stage 4	52	10.611 (5.412–20.806)	<0.001	12.565 (6.368–24.793)	
Gender	619		0.371		
Female	221	Reference			
Male	398	1.123 (0.870–1.449)	0.373		
Age	616	1.017 (1.007–1.028)	<0.01	1.025 (1.013–1.036)	<0.001

BMI: body mass index. Tumor location, tumor infiltration pattern, venous infiltration, and nerve infiltration were according to the post-operative pathology report. INFa: expanding growth and a distinct border with the surrounding tissue, INFc: infiltrating growth and an indistinct border with the surrounding tissue, INFb: in-between INFa and INFc. CEA: carcinoembryonic antigen, CA19-9: carbohydrate antigen 19-9, CA72-4: carbohydrate antigen 72-4. CEA, CA19-9, and CA72-4 were according to the tumor marker examination. Histological type, Borrmann type and pTNM stage were according to the 8th AJCC system.

Table 3. Relationship between FBLN5 mRNA expression and clinical features of GC patients.

Characteristic	High Expression	Low Expression	p
n	116	64	
Sex, n (%)			0.066
Female	24 (13.3%)	22 (12.2%)	
Male	92 (51.1%)	42 (23.3%)	
Age, n (%)			0.173
<60	59 (32.8%)	25 (13.9%)	
≥60	57 (31.7%)	39 (21.7%)	
BMI, n (%)			0.355
<24	80 (44.4%)	39 (21.7%)	
≥24	36 (20%)	25 (13.9%)	
Tumor infiltration pattern, n (%)			0.037
INFa	19 (10.6%)	17 (9.4%)	
INFb	36 (20%)	8 (4.4%)	
INFc	41 (22.8%)	27 (15%)	
N/A	20 (11.1%)	12 (6.7%)	
Lymphatic infiltration, n (%)			0.050
Negative	59 (32.8%)	43 (23.9%)	
Positive	57 (31.7%)	21 (11.7%)	
Venous infiltration, n (%)			0.209
Negative	81 (45%)	51 (28.3%)	
Positive	35 (19.4%)	13 (7.2%)	
Nerve infiltration, n (%)			0.179
Negative	26 (14.4%)	21 (11.7%)	
Positive	90 (50%)	43 (23.9%)	
T stage, n (%)			0.241
T1	6 (3.3%)	4 (2.2%)	
T2	14 (7.8%)	13 (7.2%)	
T3	42 (23.3%)	26 (14.4%)	
T4	54 (30%)	21 (11.7%)	
N stage, n (%)			0.046
N0	25 (13.9%)	25 (13.9%)	
N1	24 (13.3%)	12 (6.7%)	
N2	32 (17.8%)	9 (5%)	
N3	35 (19.4%)	18 (10%)	
pTNM stage, n (%)			0.065
I	10 (5.6%)	13 (7.2%)	
II	36 (20%)	20 (11.1%)	
III	70 (38.9%)	31 (17.2%)	
Metastatic lymph node ratio, n (%)			0.510
<0.3	87 (48.3%)	53 (29.4%)	

≥0.6	9 (5%)	3 (1.7%)	
0.3≥, <0.6	20 (11.1%)	8 (4.4%)	
Borrmann type, n (%)			0.187
1	8 (4.4%)	7 (3.9%)	
2	32 (17.8%)	17 (9.4%)	
3	62 (34.4%)	38 (21.1%)	
4	14 (7.8%)	2 (1.1%)	
Post-operative chemotherapy, n (%)			1.000
With	3 (1.7%)	1 (0.6%)	
Without	113 (62.8%)	63 (35%)	
Tumor location, n (%)			0.780
Entire stomach	4 (2.2%)	2 (1.1%)	
Lower third	65 (36.1%)	32 (17.8%)	
Middle and Upper third	47 (26.1%)	30 (16.7%)	
Histological type, n (%)			0.079
Mucinous	13 (7.2%)	5 (2.8%)	
Poorly differentiated	33 (18.3%)	11 (6.1%)	
Signet ring cell	26 (14.4%)	11 (6.1%)	
Well to moderately differentiated	44 (24.4%)	37 (20.6%)	
HER2 expression, n (%)			1.000
Negative	100 (55.6%)	55 (30.6%)	
Positive	16 (8.9%)	9 (5%)	
CEA, n (%)			0.434
>5 ng/mL	17 (9.4%)	6 (3.3%)	
≤5 ng/mL	99 (55%)	58 (32.2%)	
CA-199, n (%)			0.114
>37 U/mL	18 (10%)	4 (2.2%)	
≤37 U/mL	98 (54.4%)	60 (33.3%)	
CA724, n (%)			1.000
>6 U/mL	30 (16.7%)	17 (9.4%)	
≤6 U/mL	86 (47.8%)	47 (26.1%)	

BMI: body mass index. Tumor location, tumor infiltration pattern, venous infiltration, and nerve infiltration were according to the post-operative pathology report. INFa: expanding growth and a distinct border with the surroundinsg tissue, INFc: infiltrating growth and an indistinct border with the surrounding tissue, INFb: in-between INFa and INFc. CEA: carcinoembryonic antigen, CA19-9: carbohydrate antigen 19-9, CA72-4: carbohydrate antigen 72-4. CEA, CA19-9, and CA72-4 were according to the tumor marker examination. Histological type, Borrmann type and pTNM stage were according to the 8th AJCC system.

FBLN5 across different cancer types

The results above indicate that FBLN5 serves as a reliable prognostic marker in gastric cancer. We extended this analysis to examine whether FBLN5 could predict outcomes in other malignancies by evaluating its expression levels in multiple cancer types and correlating them with patient prognosis. The findings suggested that FBLN5 expression is also prognostically relevant in hepatocellular carcinoma, highlighting its potential clinical utility in this context **(Figures 7a and 7b)**.

Furthermore, we investigated the relationship between FBLN5 expression and immune cell infiltration across diverse cancers using TIMER and CIBERSORT algorithms. TIMER analysis indicated a generally positive correlation between FBLN5 levels and immune cell infiltration in most tumor types **(Figure 7c)**, whereas CIBERSORT revealed predominantly negative associations **(Figure 7d)**, suggesting that the impact of FBLN5 on tumor immunity may vary by cancer type and requires further exploration.

We also assessed the association between FBLN5 expression and immune checkpoint markers, finding positive correlations in several cancers, including lung adenocarcinoma (STES), bladder transitional cell carcinoma (BLCA), and lung squamous cell carcinoma (LUSC), which may inform potential immunotherapy strategies **(Figure 7e)**.

Lastly, we evaluated the pan-cancer implications of FBLN5 for targeted therapy by analyzing tumor purity (**Figure 7f)**, tumor mutational burden (TMB) **(Figure 7g)**, and microsatellite instability (MSI) **(Figure 7h)**. High FBLN5 expression generally correlated negatively with TMB and MSI, suggesting limited efficacy of targeted therapy in such cases. Collectively, FBLN5 appears to exhibit context-dependent roles, promoting or suppressing

tumor progression depending on the cancer type, and may influence responsiveness to immunotherapy and targeted therapy. These findings underscore the need for tumor-specific investigations into the mechanistic functions of FBLN5.

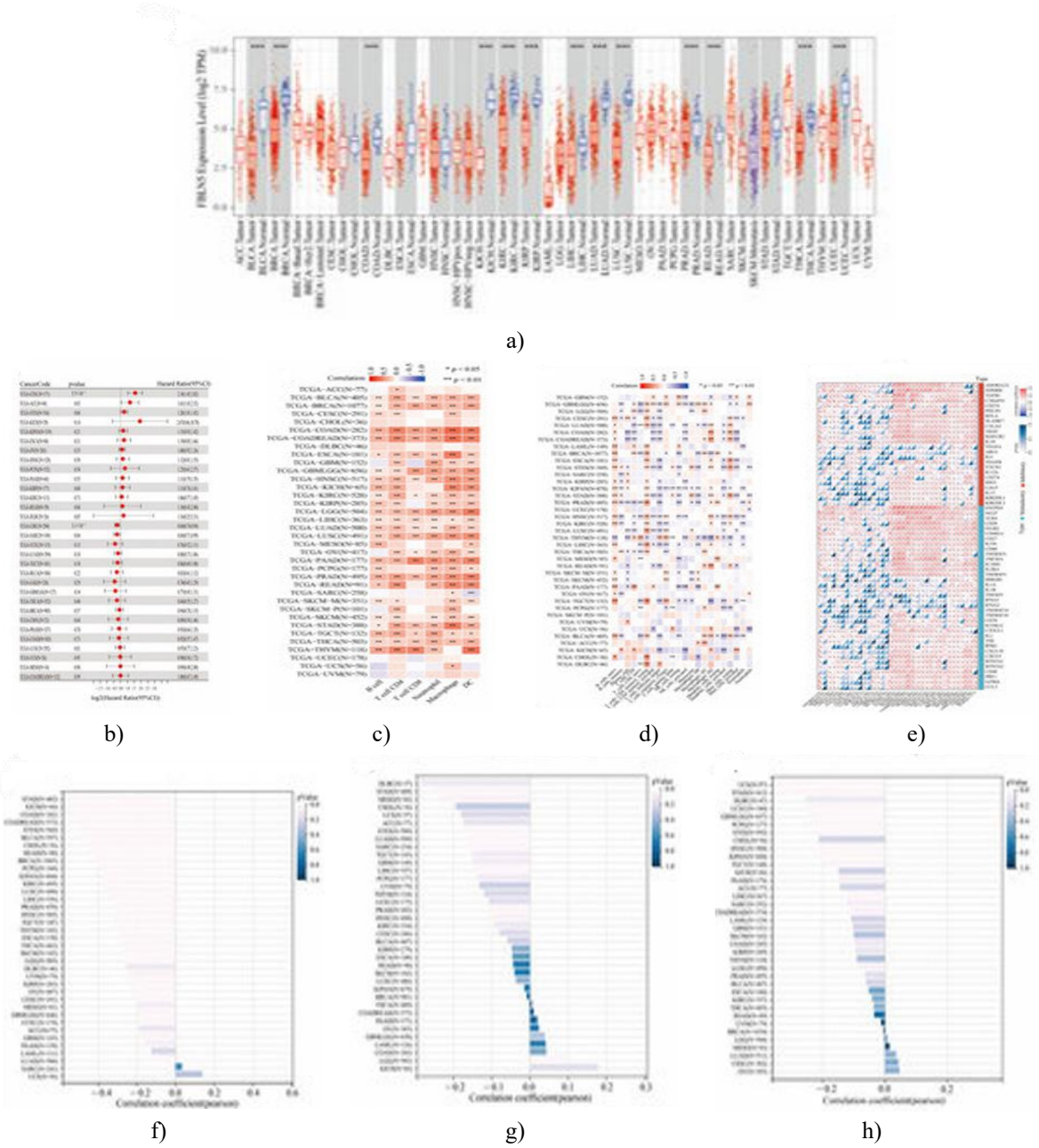

Figure 7. Application of FBLN5 in other cancers. (a) Expression levels of FBLN5 in various cancers. (b) Prognostic analysis of FBLN5 in various cancers. (c) TIMER algorithm and (d) CIBERSORT algorithm preliminarily predicted the relationship between the expression level of FBLN5 and immune infiltration in various types of tumors. (e) Pan-cancer analysis of FBLN5-related immune checkpoints, along with (F) tumor purity, (g) TMB, and (h) MSI analyses to evaluate the prospect of using FBLN5 for targeted pan-cancer treatment. * $p < 0.05$, ** $p < 0.01$, *** $p < 0.001$.

Discussion

Gastric cancer (GC) is a highly aggressive malignancy of the digestive tract, characterized by a complex tumor microenvironment (TME). In this study, we utilized TCGA-HMU GC datasets to investigate the biological functions of FBLN5 in GC, examining its mRNA and protein expression levels and their associations with clinicopathological features and patient outcomes. Our findings suggest that FBLN5 plays a key role within the TME and may serve as a prognostic biomarker linked to tumor-associated fibroblast activity.

Fibulins comprise a family of seven extracellular matrix proteins (fibulin-1 to fibulin-7) that participate in diverse biological processes, including cell adhesion, migration, and proliferation. They are widely expressed in both vascular and elastic tissues and are involved in modulating tumor progression through their activity in both tumor and stromal cells [26]. FBLN5, a fibroblast-derived ECM protein, contains an Arg-Gly-Asp (RGD) motif and calcium-binding EGF-like domains, enabling it to mediate endothelial cell adhesion through integrin interactions. Beyond its critical role in elastic fiber assembly [14], FBLN5 contributes to vascular development and remodeling [12] and interacts with TGF-β in fibroblasts and endothelial cells [16, 17], linking it to pathological processes such as EMT during fibrosis and tumorigenesis [27, 28]. Prior studies have reported that FBLN5 promotes EMT via matrix metalloproteinase-dependent mechanisms in breast cancer [29] and enhances pancreatic cancer progression by modulating the ECM and reactive oxygen species generation [21]. However, its clinical relevance in GC has remained largely unexplored.

In our study, PCA analysis demonstrated good intra-group consistency, although the separation between high- and low-expression groups was modest, likely due to the continuous nature of FBLN5 expression. Elevated FBLN5 levels were significantly associated with T stage, N stage, and pTNM stage, with expression increasing alongside tumor progression and lymph node involvement, correlating with worse prognosis. These observations are consistent with findings in other malignancies where tumor-associated fibroblast abundance correlates with disease stage and outcomes [30].

Functional enrichment analyses revealed that FBLN5 was primarily involved in the MAPK signaling pathway. Previous research has demonstrated that modulation of FBLN5 can influence the MAPK/ERK pathway, affecting tumor progression [31], while interactions with LOXL1 promote angiogenesis and metastasis via the LOXL1-FBLN5/integrin/FAK-MAPK axis [32]. GSEA further indicated that high FBLN5 expression was linked to TGF-β signaling, EMT, apoptosis, hypoxia, and angiogenesis pathways, highlighting its integral role in the TME and in facilitating tumor metastasis. Similar mechanistic roles of FBLN5 have been reported in breast and pancreatic cancers, where it enhances TGF-β-induced EMT and is upregulated under hypoxic conditions, contributing to poor prognosis [20, 21]. FBLN5 has also been directly associated with angiogenic processes [33], suggesting that its overexpression in GC may drive poor outcomes through coordinated activation of hypoxia, angiogenesis, MAPK signaling, EMT, and TGF-β pathways.

Through protein-protein interaction network analysis, we identified ELN as a key interacting partner of FBLN5. Previous studies from our group showed that ELN expression correlates positively with fibroblast markers, particularly VIM, and may serve as a prognostic indicator in GC by regulating EMT [34]. This suggests that FBLN5 could influence tumor progression in GC not only through intrinsic tumor cell mechanisms but also by modulating fibroblast activity within the TME.

Richard *et al*. [9] described CAFs and the ECM collectively as "stromal," which can suppress immune cell activity and contribute to tumor initiation, progression, metastasis, and therapy resistance. Given that FBLN5 is a fibroblast-derived extracellular matrix protein, we hypothesized that it may similarly inhibit immune cell function and facilitate tumor immune escape. CIBERSORT analysis revealed that overexpression of FBLN5 was associated with increased infiltration of M2 macrophages and dendritic cells, suggesting that high FBLN5 expression may be linked to the presence of immunosuppressive cell populations, including CAFs, tumor-associated macrophages (TAMs), and dendritic cells. M2 macrophages, characterized by elevated IL-10, VEGF, and MMP expression, contribute to angiogenesis, tissue remodeling, and tumor progression, while exerting immunosuppressive effects [35, 36]. Similarly, tumor-associated dendritic cells can secrete factors that promote regulatory T-cell proliferation and angiogenesis, further suppressing antitumor immunity. Patients with high FBLN5 expression also exhibited elevated immune, stromal, and ESTIMATE scores, along with reduced tumor purity, indicating a TME enriched with fibroblasts that may promote immunosuppression. These findings highlight the importance of further investigating the relationship between FBLN5 and immune infiltration.

Clinically, Chi-square analysis showed significant associations between FBLN5 expression, the INFc tumor infiltration pattern, and N3 stage. Zhao *et al*. [37] reported that the INFc pattern correlates with deep tumor invasion, immunosuppression, and poor differentiation, all of which predict adverse outcomes. Correspondingly, higher lymph node involvement was associated with poorer prognosis, suggesting that elevated FBLN5 may indicate advanced GC. Cox univariate and multivariate analyses confirmed that FBLN5 expression and lymph node metastasis were independent prognostic factors. The relatively limited number of independent predictors in our study may reflect the small cohort size (180 patients, with only 100 having adequate follow-up) and the generally short survival duration in GC. Based on these findings, we developed a nomogram combining FBLN5

expression and lymph node metastasis to predict patient prognosis. The model demonstrated a C-index of 0.705 (0.659–0.752), with AUCs of 0.751, 0.769, and 0.733 for one-, two-, and three-year survival predictions, respectively. These results underscore the potential clinical and research utility of FBLN5 as a prognostic marker. We also investigated the role of FBLN5 in other cancers using bioinformatics analyses. Notably, FBLN5 expression was predictive of prognosis in hepatocellular carcinoma, where lower expression correlated with poorer survival [38]. Mechanistically, FBLN5 appears to inhibit hepatocellular carcinoma cell motility through integrin-dependent pathways, and RGD-mediated suppression of MMP-7 may inform novel therapeutic strategies. Furthermore, in cancers such as STES, BLCA, and LUSC, FBLN5 expression could guide decisions regarding immunotherapy or targeted therapy, enabling more personalized treatment approaches and potentially improving patient outcomes and quality of life.

Several limitations should be acknowledged. First, gene expression and IHC data were derived from separate cohorts, making integration of multi-omics data challenging. Second, the study cohort was relatively small. Third, functional cellular experiments are critical for validating prognostic biomarkers, yet our study relied primarily on bioinformatics analyses, with experimental validation limited to proliferation, migration, and invasion assessments.

Conclusion

In summary, FBLN5 expression was significantly elevated in GC tissues compared with adjacent normal tissues. High FBLN5 mRNA and protein levels were associated with poorer prognosis, as well as INFc tumor infiltration and lymph node metastasis. Both FBLN5 expression and lymph node metastasis were independent prognostic factors and could be combined into a nomogram to assess patient outcomes. These findings indicate that FBLN5 is a valuable prognostic biomarker for GC.

Acknowledgments: None

Conflict of Interest: None

Financial Support: This work was partially supported by the Natural Science Foundation of Inner Mongolia Autonomous Region: 2022QR08003 (Shengjie Yin).

Ethics Statement: The study was conducted in accordance with the Declaration of Helsinki and approved by the Ethics Committee from Harbin Medical University Cancer Hospital, China (Approval Number: SHGC-1029). Informed consent was obtained from all subjects involved in the study.

References

1. Ajani JA, D'Amico TA, Bentrem DJ, Chao J, Cooke D, Corvera C, et al. Gastric cancer, version 2.2022, NCCN clinical practice guidelines in oncology. J Natl Compr Canc Netw. 2022;20(2):167–92.
2. Digklia A, Wagner AD. Advanced gastric cancer: current treatment landscape and future perspectives. World J Gastroenterol. 2016;22(8):2403–14.
3. Yang Y, Meng WJ, Wang ZQ. Cancer stem cells and the tumor microenvironment in gastric cancer. Front Oncol. 2021;11:803974.
4. Yago A, Haruta S, Ueno M, Hamada Y, Ogawa Y, Ohkura Y, et al. Adequate period of surveillance in each stage for curatively resected gastric cancer. Gastric Cancer. 2021;24(4):752–61.
5. Unterleuthner D, Neuhold P, Schwarz K, Janker L, Neuditschko B, Nivarthi H, et al. Cancer-associated fibroblast-derived WNT2 increases tumor angiogenesis in colon cancer. Angiogenesis. 2020;23(2):159–77.
6. Zhuang J, Lu Q, Shen B, Huang X, Shen L, Zheng X, et al. TGFβ1 secreted by cancer-associated fibroblasts induces epithelial–mesenchymal transition of bladder cancer cells through lncRNA-ZEB2NAT. Sci Rep. 2015;5:11924.
7. Oft M, Akhurst RJ, Balmain A. Metastasis is driven by sequential elevation of H-Ras and Smad2 levels. Nat Cell Biol. 2002;4(7):487–94.
8. Yan Y, Wang LF, Wang RF. Role of cancer-associated fibroblasts in invasion and metastasis of gastric cancer. World J Gastroenterol. 2015;21(28):9717–26.

9. Barrett RL, Puré E. Cancer-associated fibroblasts and their influence on tumor immunity and immunotherapy. eLife. 2020;9:e57243.
10. Timpl R, Sasaki T, Kostka G, Chu ML. Fibulins: a versatile family of extracellular matrix proteins. Nat Rev Mol Cell Biol. 2003;4(6):479–89.
11. Argraves WS, Greene LM, Cooley MA, Gallagher WM. Fibulins: physiological and disease perspectives. EMBO Rep. 2003;4(12):1127–31.
12. Nakamura T, Ruiz-Lozano P, Lindner V, Yabe D, Taniwaki M, Furukawa Y, et al. DANCE, a novel secreted RGD protein expressed in arteries. J Biol Chem. 1999;274(32):22476–83.
13. Nakamura T, Lozano PR, Ikeda Y, Iwanaga Y, Hinek A, Minamisawa S, et al. Fibulin-5/DANCE is essential for elastogenesis in vivo. Nature. 2002;415(6868):171–5.
14. Claus S, Fischer J, Mégarbané H, Mégarbané A, Jobard F, Debret R, et al. A p.C217R mutation in Fibulin-5… J Investig Dermatol. 2008;128(6):1442–50.
15. Heo JH, Song JY, Jeong JY, Kim G, Kim TH, Kang H, et al. Fibulin-5 is a tumour suppressor inhibiting cell migration and invasion in ovarian cancer. J Clin Pathol. 2016;69(2):109–16.
16. Schiemann WP, Blobe GC, Kalume DE, Pandey A, Lodish HF. Context-specific effects of Fibulin-5. J Biol Chem. 2002;277(30):27367–77.
17. Albig AR, Schiemann WP. Fibulin-5 antagonizes VEGF signalling and angiogenic sprouting. DNA Cell Biol. 2004;23(6):367–79.
18. Hu Z, Ai Q, Xu H, Ma X, Li HZ, Shi TP, et al. Fibulin-5 is down-regulated in urothelial carcinoma. Urol Oncol. 2011;29(4):430–5.
19. Chen X, Song X, Yue W, Chen D, Yu J, Yao Z, et al. Fibulin-5 inhibits Wnt/β-catenin signalling in lung cancer. Oncotarget. 2015;6(16):15022–34.
20. Lee YH, Albig AR, Regner M, Schiemann BJ, Schiemann WP. Fibulin-5 initiates EMT and enhances TGF-β-induced EMT. Carcinogenesis. 2008;29(12):2243–51.
21. Topalovski M, Hagopian M, Wang M, Brekken RA. Hypoxia and TGF-β induce Fibulin-5 expression in pancreatic cancer. J Biol Chem. 2016;291(43):22244–52.
22. Xiao W, Zhou S, Xu H, Li H, He G, Liu Y, et al. Nogo-B promotes EMT via Fibulin-5. Oncol Rep. 2022;47(1):100.
23. Effect of Fibulin-5 on cell proliferation and invasion in human gastric cancer. Available from: https://pubmed.ncbi.nlm.nih.gov/25129461/.
24. Wang X, Zhi Q, Liu S, Xue SL, Shen C, Li Y, et al. Identification of biomarkers for gastric adenocarcinoma by iTRAQ. Sci Rep. 2016;6:38871.
25. Shen W, Song Z, Zhong X, Huang M, Shen D, Gao P, et al. Sangerbox: a comprehensive clinical bioinformatics platform. iMeta. 2022;1:e36.
26. Obaya AJ, Rua S, Moncada-Pazos A, Cal S. The dual role of fibulins in tumorigenesis. Cancer Lett. 2012;325(1):132–8.
27. Galliher AJ, Neil JR, Schiemann WP. Role of TGF-β in cancer progression. Future Oncol. 2006;2(6):743–63.
28. Nawshad A, Lagamba D, Polad A, Hay ED. TGF-β signalling during EMT. Cells Tissues Organs. 2005;179(1):11–23.
29. Manders DB, Kishore HA, Gazdar AF, Keller PW, Tsunezumi J, Yanagisawa H, et al. Dysregulation of Fibulin-5 in ovarian cancer. Oncotarget. 2018;9(20):14251–67.
30. Dourado MR, Guerra ENS, Salo T, Lambert DW, Coletta RD. Prognostic value of CAF detection in oral cancer. J Oral Pathol Med. 2018;47(5):443–53.
31. Li Y, Yang X, Lu D. Knockdown of UBE2T suppresses lung adenocarcinoma via Fibulin-5. Bioengineered. 2022;13(5):11867–80.
32. LOXL1 promotes oncogenesis via LOXL1-FBLN5/integrin pathway. Available at: https://pubmed.ncbi.nlm.nih.gov/33614230/.
33. Yoshida K, Nagasaka T, Umeda Y, Tanaka T, Kimura K, Taniguchi F, et al. EFEMP1 promoter alterations and malignancy. J Cancer Res Clin Oncol. 2016;142(7):1557–69.
34. Fang T, Zhang L, Yin X, Wang Y, Zhang X, Bian X, et al. Elastin correlates with EMT in gastric cancer. J Pathol Clin Res. 2022;9(1):56-72.

35. Belgiovine C, D'Incalci M, Allavena P, Frapolli R. Tumor-associated macrophages and anti-tumor therapies. Cell Mol Life Sci. 2016;73(13):2411–24.
36. Pan Y, Yu Y, Wang X, Zhang T. Tumor-associated macrophages in tumor immunity. Front Immunol. 2020;11:583084.
37. Tumor infiltrative growth pattern and immune microenvironment. Available at: https://pubmed.ncbi.nlm.nih.gov/32232560/.
38. Tang JC, Liu JH, Liu XL, Liang X, Cai XJ. Effect of Fibulin-5 on adhesion and invasion of hepatocellular carcinoma. World J Gastroenterol. 2015;21(39):11127–40.